Title
Tunable nano bead arrays on film for controlling propogation of light

ISBN
9780819496591

Authors
Sharac, Nicholas
Sharma, Himanshu
Khine, Michelle
et al.

Publication Date
2013-09-11

DOI
10.1117/12.2026143

Tunable nano bead arrays on film for controlling propogation of light

Nicholas Sharac[1*], Himanshu Sharma[3*], Michelle Khine[3], Regina Ragan[2]

[1]*Department of Chemistry, University of California Irvine, CA, 92697 USA*
[2]*Department of Chemical Engineering & Materials Science, University of California Irvine, CA, 92697 USA*
[3]*Department of Biomedical Engineering, University of California Irvine, CA, 92697 USA*

ABSTRACT

Periodic arrays of sub-wavelength structures have garnered significant interest for surface enhanced Raman spectroscopy (SERS) and metal enhanced fluorescence (MEF), and for anti-reflective coating properties. For SERS and MEF, coupling metal nanoparticles with nanometer scale spacing can induce strong local electromagnetic field enhancements at the plasmon resonance, significantly increasing the Raman signal or fluorescence of a molecule. Inspired by moth eyes, metal nanoparticle arrays can reduce the reflection of incident light, shown useful for improving the efficiency of solar cells. Here, we present fabrication of robust, tunable, inexpensive and quickly reproducible gold coated, nanopillar arrays for applications in enhancing Raman/fluorescence signals or anti-reflective surfaces for efficient solar cells. To create homogenous metallic nanostructures with controllable sizes and interparticle spacings, we have integrated conventional nanosphere lithography techniques with thermally responsive polyolefin (PO) films. Spin coating 500 nm PS beads onto PO substrates, followed by oxygen plasma etching, is used to vary the size and periodicity of the resulting PS nanopillar bead array. A 50 nm thick gold film can then be added using chemical vapor deposition (CVD). Nanostructures were characterized with scanning electron microscopy and atomic force microscopy. When heated from room temperature up to 115^{o}C, structures on PO films undergo a reduction in feature size and interparticle spacing by up to 35 % in length and 50% in surface area.

Keywords: nanosphere lithography, nanophotonics, bottom up lithography, thermal substrate, plasmonics.

1. INTRODUCTION

Tuning the localized surface plasmon resonance in noble metal structures is pivotal in optimizing a wide range of applications, such as nanophotonic devices[1,2,3,4,5,6], biological sensors[7,8], and photovoltaics.[9] The highest enhancement factors for surface enhanced Raman spectroscopy (SERS)[10] and metal enhanced fluorescence (MEF)[11], currently greater than 1x10^9[12] and 1,100 fold[13],respectively, are attained when the plasmon frequency is between the frequency of the incident light and that of the light emitted from the analyte molecule.[14,15] For solar cell devices, enhancing light absorption in the solar frequency range allows for the highest increases in efficiency.[16] Additionally, dielectric structures with anti-reflective (AR) properties have shown promise in increasing absorption for solar cells and transmittance for light-emitting diodes (LED).[17] The AR properties arise from periodic structures smaller than the wavelength of light, which results in a smooth gradient in the refractive index and an effective absence of an air lens interface.[18]

Plasmonics: Metallic Nanostructures and Their Optical Properties XI, edited by Mark I. Stockman,
Proc. of SPIE Vol. 8809, 88091O · © 2013 SPIE · CCC code: 0277-786X/13/$18 · doi: 10.1117/12.2026143

Control over materials, size, shape, and periodicity of nanostructures, all variables in tuning the resonance frequency, has largely been attained via top down methods, such as electron beam lithography[19], dip pen lithography[20], and focused ion beam lithography[21]. For instance, Caldwell et all, has used e-beam lithography to generate gold nanopillar arrays, with diameters ranging from 320 nm to 120 nm and distances from 270 nm to 60 nm, with uniform enhancement factors as high as ~1.2x10^8.[22] However, these traditional top down methods are not realizable commercially, due to high cost, long process time, and low throughput. Bottom down methods, such as nanosphere lithography (NSL)[23], offer more robust, cheaper solutions, with higher coverage, but at the cost of versatility. In work by Lim[18], nano pillar arrays, in close resemblance to the cones in a moth's eye, were fabricated on both sides of glass using NSL, resulting in a 99% transparency in the visible region.[18] By tuning the height and pillar shape, they were able to tune the frequency region in which the AR properties occurred. However, the spacing between pillars, which plays a direct role in the refractive index gradient, remained fixed, due to the inherent inability of NSL to alter periodicity independently of structure height and size. Ideally, new techniques which combine the best of both top down and bottom methods should be explored.

In this work, we have developed a low cost, robust, high throughput and versatile technique to fabricate arrays of nanostructures. We are able to produce nanopillar arrays similar to the work done by Caldwell and by Lim, but with the added benefit of increased tunability. By combining NSL, which generates a hexagonal closed pack array of polymer beads from several microns down to 200 nm on a surface, with a polyolefin film (PO), a reduction in surface area of up to 95% and 77% in length[24] is attainable. Plasma etching supplies another independent parameter to vary the size of PS and the height of nano bead-pillars. The process is shown in figure 1. NSL provides a hexagonal closed pack mask of latex beads of 500 nm diameter. Introducing the beads and PO substrate to oxygen plasma allows for tuning of the beads diameter and spacing in addition to creation of pillar structures from the etched PO. The substrate, consisting of a polyolefin blend, is pre-stressed, and therefore reduces in surface area when exposed to temperatures above 100°C. This is used to modify the geometry of our pillar array. Overall the spacing, feature size and height of these nano pillars can be tuned independently by thermal processing and plasma etching. Finally, gold can be added to our pillars via chemical vapor deposition (CVD).

2. EXPERIMENTAL

Polyolefin (PO) films (955-D, Sealed Air Corporation) ,with thickness of approximately 1 millimeter, that are laminated on a 3 millimeter polyester backing, are cleaned in isopropyl alcohol and then dried with pressurized air. The clean PO film is then oxygen plasma treated for 30 s at a power of 60 W to increase the hydrophilicity of PO surfaces. A solution of 500 nm polystyrene (PS) beads (Bangs lab) was diluted to a 3:1 ratio with triton X-100 and methanol (1:400 by volume). Approximately 12 µL of this solution was then spin coated onto the PO film for 5 minutes at 1000 RPM and allowed to dry for two hours. After spin coating, the substrate was plasma etched at a power of 60 W in an Oxygen plasma asher for different times, from 540 s to 810 s. Immediately following the plasma etch step, samples were sonicated in ethanol for one minute and subsequently sonicated in deionized (DI) water for thirty seconds to remove residual etchant material. The samples were then mounted on a glass slide with double sided tape and heated in a convection oven from room temperature to different degrees of temperature ranging from 90°C to 120°C. The differences in the length from the original PO size were measured with a digital caliper during the heating process. The percentages shrunk in length were calculated by taking the ratio of the final width of substrate relative to the initial width. Finally, samples were coated with a 5 nm titanium adhesion layer and 50 nm Au, using chemical vapor deposition. Temperatures did not exceed 115° C during this process to avoid further shrinking. An atomic force microscope (AFM) (Asylum Research MFP-3D AFM) with silicon cantilevers (Olympus) was used to characterize the resulting topography of our substrate, and a scanning electron microscope (SEM) (FEI- Magellan 400 L XHR), at ~ 2 kv, was used to image the periodicity of features over a large area.

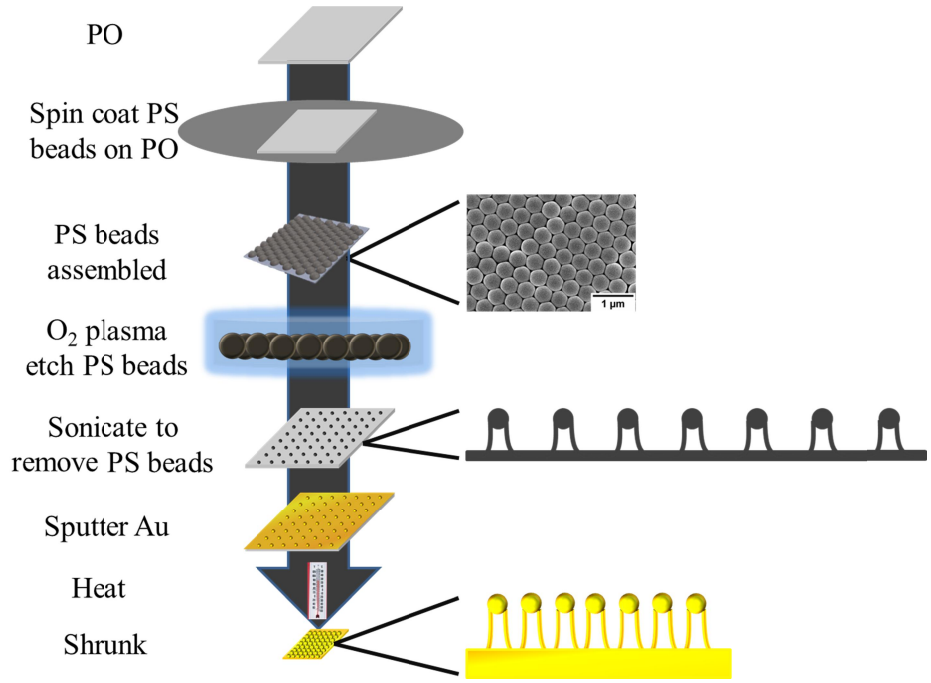

Figure 1. Schematic process flow for fabrication of nanopillar bead arrays.

3. RESULTS

The oxygen plasma etch time was varied to determine the etch rate of PS beads and the underlying PO. SEM images after etching are shown in Figure 2 a-d, etched for time periods of (a) 540 s, (b) 630 s, (c) 720 s, (d) 810 s, respectively, since plasma etching the PS beads was found to be most effective in this time range. Etching times less than 540 s resulted in minimal etching of PS beads, and beyond 810 s, the pillars were found to be damaged in SEM images, data not shown. Etching for time periods of 540-810 s led to a deformation of PS beads, as observed in figure 2. Etch times longer than 810 s led to significant etching of PS beads to the point of obliteration. Figure 2d, shows the PS beads to be significantly smaller and distorted when compared to Figures 2a, 2b and 2c. As expected, as the diameter of nanopillars is reduced due to increasing the etch time, the inter-spacing between the pillars is increased as observed in Figure 2 a-d. As the measured pillar width decreased from approximately 240 nm to 100 nm, when the etch time increased from 540 to 810 s, the edge to edge spacing increased from approximately 250 nm to 400 nm. AFM topography line profiles are shown in Figure 2e and 2f, corresponding to etch times of 540s and 810 s, respectively. The height profiles illustrate that with longer etch times, the top point of the pillars becomes sharper relative to the smooth tops observed on pillars after an etch time of 540 s, observed in both in Fig. 2e and 2f.

AFM topography images of the etched beads are shown in the first row of Figure 3, with a common height scale legend on the right, show that heights range from approximately 60 nm for pillars etched for 540 s and up to 160 nm for an plasma etch time of 810 s and the height increase is monotonic with etch time. Due to the diminished beads after 810s of plasma etching, while the etched PO film was still intact, further deepening of the pillar features on the surface was not possible due to the obliteration of the PS NSL mask. If a higher aspect ratio is needed, RIE can be used, due to the difference in dry etch rates between PO and PS. [25,26] This is especially important for plasmonic applications where high aspect ratio structures are correlated with strong local electric fields[27] or for anti-reflection applications such as "moth eye" structures, where height has been shown to play a major role in AR, due

to suppression of light reflection.[28] Traditionally, NSL has been performed on Si substrates to generate pillars with heights up to 400 nm by using selective etching methods, such as RIE, with fluorination or chemical etchants.[29] On such a hard surface, the beads do not adhere to the surface and are removed after sonication in a solvent. Using a soft PO film, the PS beads remain bound to the PO film surface. Also, the beads appeared to have a strong adhesion to the PO surface. Sonicating the PS coated PO films in organic solvents such as hexanes and dichloromethane did not lead to release of PS beads. If combined with selective etching, tall, high aspect pillars can be attained with easily shapeable caps.

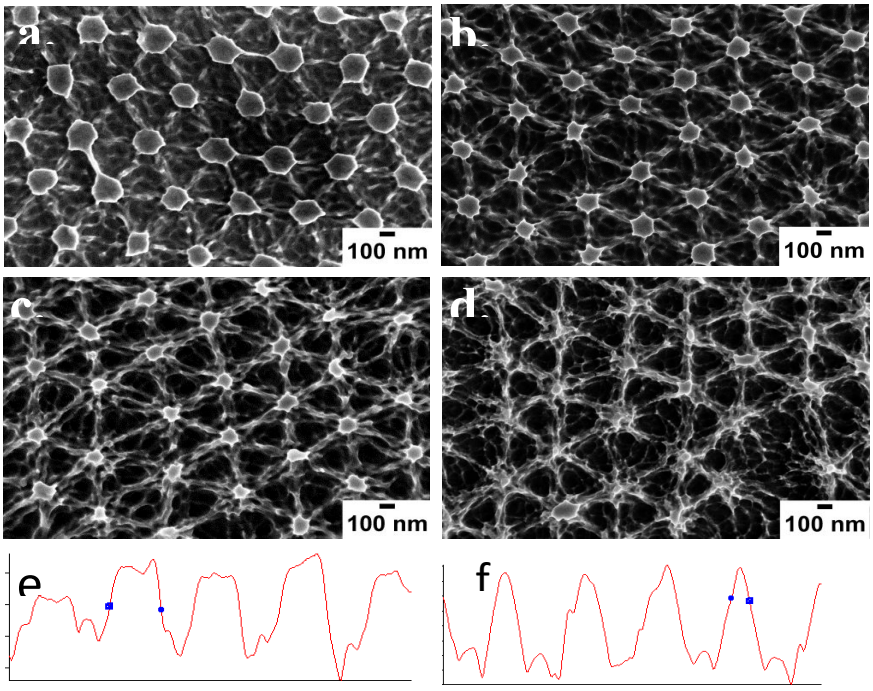

Figure 2. SEM images of gold coated 500 nm PS bead arrays that were reduced in size using various plasma etch times: a. 540 s, b. 630 s, c. 730 s, d. 810 s. Scale bar is 100 nm. 2 µm AFM height profiles for samples etched for e. 540 s, and f. 810 s provide the shape of the resulting nanopillar beads.

We also investigated how a combination of etching and thermal processing leads to independent control of feature size and periodicity not obtained in conventional NSL. Figure 3 shows AFM topography images for PS bead arrays on PO, etched for different durations and heated from room temperature to 105° C and 115°C. Visually, it can be observed in the AFM images that as the substrate is heated, the spacing between nanopillars decreases. This decrease is correlated with the percentage of decrease in dimensions of the PO substrate. Furthermore, thermal processing also increases the heights of the nano bead pillars by approximately 30 nm when heated to 115°C. Based on the conservation of mass law, since the PO contracts in the X and Y direction, the film must increase in the Z direction. Approximately 30 nm increase in the height was observed when shrinking to approximately 35% in length for all the etch times. Although the PO film has the ability to contract by up to77% in length by heating to 155°C, the substrates were only shrunk to approximately 35% in length at T = 115 °C. The limit in thermal processing and achievable reduction in feature size, as has been previously demonstrated, is due to stiffening of the PO surface during etching. With the addition of the thin oxide layer during plasma etching and metal deposition, shrinking the PO film past 35% in length forced wrinkles to form. This was clearly evident in the SEM and AFM images where the bead pillar arrays became masked by the wrinkles or the features were not all in one plane. A summary of the

differences in the widths, heights, and distances measured for the substrates is presented in Table 1. For a more quantitative analysis, the same values are also plotted as a function of etch time shown in Figure 4. It is important to note that the spacings reported were measured from center to center, and therefore no decrease in distance as a function of etch time is shown here.

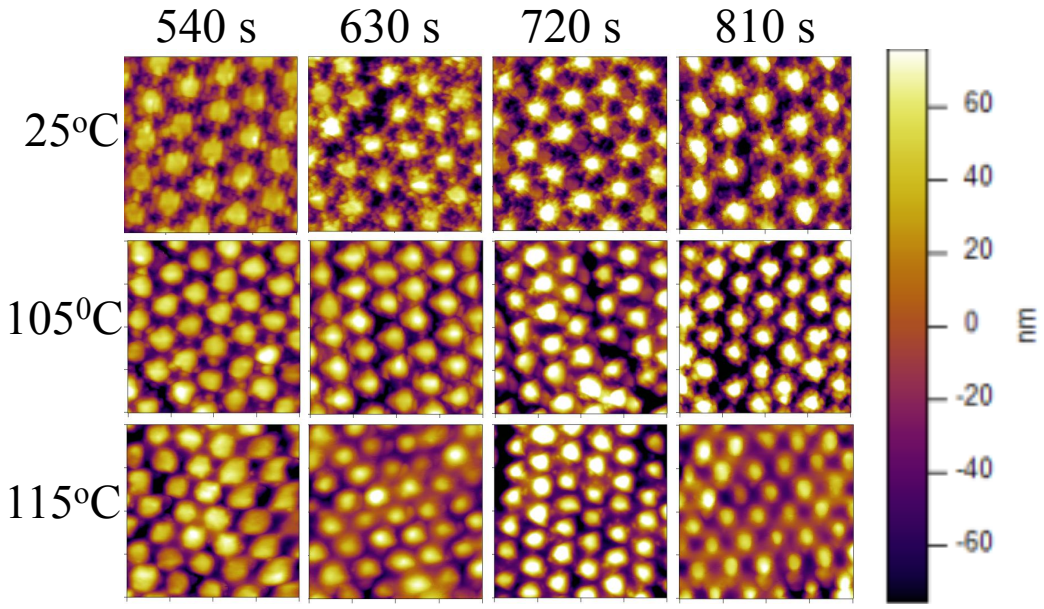

Figure 3. AFM topography images of gold coated 500 nm PS bead arrays on PO, etched for different time intervals and then shrunk in size from 0% to 20% to 33% by heating them from 25°C to 105°C to 115°C, respectively.

As presented in Table 1 and illustrated in Figure 4, the nanopillars do not vary much in width after heating. In theory, shrinking the substrates should result in smaller diameter of the pillars. This may be related to the PO being segmented into small areas when etched into pillars, preventing the normal shrinking expected. As shown in figure 4, only the largest measured pillars appear to shrink to a small extent with increase in temperature. This may be due to the segmented PO still being large enough to decrease in surface area to some small extent. As expected, the center to center spacings decreased as a function of heat, as shown in table 1 and figure 4, from approximately 450 to 300 nm, which is approximately a 35% reduction in distance. This reduction in spacing corresponds well to the measured reduction in the length of our plastic substrates. Figure 4 also shows some variation exists in shrinking in the x and y directions of the substrate, which can be attributed to asymmetric stretching of the substrate. Achieving control over this asymmetry is possible by constraining the sample in one direction while heating. The constrained side can be alternated according to desired shrink percentage and desired level of asymmetry. Control of the asymmetry will allow more tunability in nanostructure arrays, in addition to keeping the periodicity consistent. An interesting observation to note is that the samples etched for 810 s showed a continual decrease in the variation of periodicity for the x and y directions as heat was increased.

Etch time (s)	Shrink Temp (°C)	Width (nm)	Spacing in x (nm)	Spacing in y (nm)	Height (nm)
540	25	237 ± 6	452 ± 11	448 ± 10	65 ± 4
540	105	224 ± 5	366 ± 10	384 10	79 ± 3

540	115	215 ± 14	314 ± 9	375 ± 15	85 ± 4
630	25	123 ± 7	451 ± 14	429 ± 19	100 ± 6
630	105	118 ± 7	381. ± 4	376 ± 5	120 ± 7
630	115	119 ± 9	314 ± 4	351 ± 6	125 ± 4
720	25	128 ± 8	438 ± 12	445 ± 10	97 ± 5
720	105	128 ± 4	381 ± 9	380 ± 10	105 ± 6
720	115	126 ± 2	343 ± 10	294 ± 9	113 ± 4
810	25	95 ± 7	439 ± 11	452 ± 9	124 ± 5
810	105	97 ± 5	386 ± 7	356 ± 6	132 ± 4
810	115	92 ± 7	320 ± 11	330 ± 8	143 ± 6

Table 1. Gap spacing and width dimensions of PS bead arrays for different etch times and shrink temperatures.

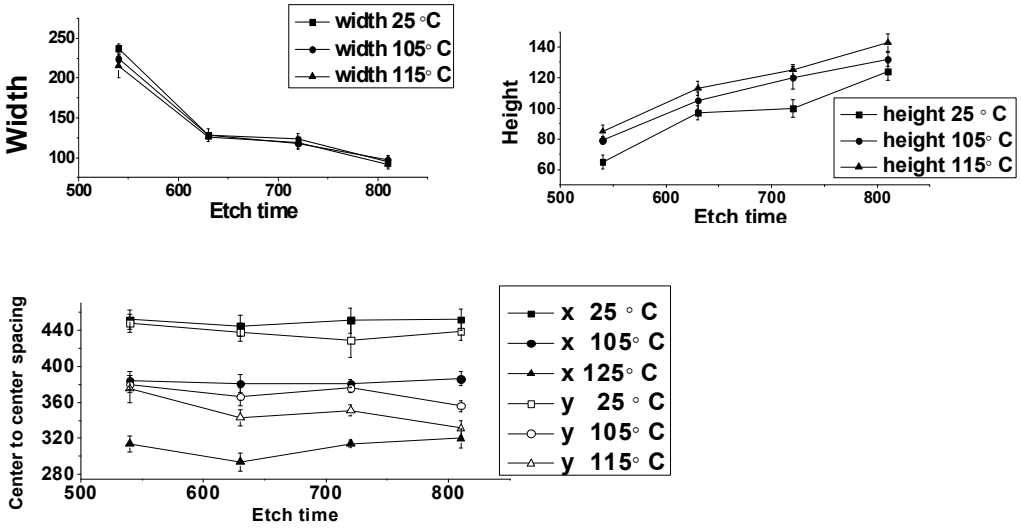

Figure 4. Spacing, width, and heights for PS bead arrays shown as a function of etch time and shrink temperatures.

4. CONCLUSION

In summary, we have developed a versatile method for quick, robust, and inexpensive fabrication of metal-dielectric nanopillar structures. The thermoplastic PO substrate allows for facile tunability of inter particle spacing and height of our structures. Thermoplastics, combined with etching, allows for us to attain a wide range of pillar widths and inter-pillar spacings. Currently, wrinkling prevents the substrates from shrinking past 35%, but this may be circumvented by first removing the oxide layer or by using a different heat film. Other etch methods, such as RIE, will be used in the future to create a deeper etch, resulting in taller pillars more suitable to AR properties. High aspect ratios in conjunction with increased height from shrinking, change in shape, and controlled variability in spacing should allow for the extensive study of AR properties in moth wing structures. Additionally, since we have deposited gold our substrates, we will next explore plasmonic effects, to be used in both SERS and MEF.

[1] J.-Q. Xi, M. F. Schubert, J. K. Kim, E. F. Schubert, M. Chen, S.-Y. Lin, W. Liu, and J. A. Smart, "Optical thin-film materials with low refractive index for broadband elimination of Fresnel reflection," *Nat Photon*, vol. 1, no. 3, pp. 176–179, Mar. 2007.

[2] S. A. Maier, “Plasmonics: Metal Nanostructures for Subwavelength Photonic Devices,” *IEEE Journal of Selected Topics in Quantum Electronics*, vol. 12, no. 6, pp. 1214–1220, 2006.
[3] E. Ozbay, “Plasmonics: Merging Photonics and Electronics at Nanoscale Dimensions,” *Science*, vol. 311, no. 5758, pp. 189–193, 2006.
[4] S. A. Maier, “Plasmonics: The Promise of Highly Integrated Optical Devices,” *IEEE Journal of Selected Topics in Quantum Electronics*, vol. 12, no. 6, pp. 1671–1677, 2006.
[5] S. Lal, S. Link, and N. J. Halas, “Nano-optics from sensing to waveguiding,” *Nat Photon*, vol. 1, no. 11, pp. 641–648, Nov. 2007.
[6] S. A. Maier, P. E. Barclay, T. J. Johnson, M. D. Friedman, and O. Painter, “Low-loss fiber accessible plasmon waveguide for planar energy guiding and sensing,” *Applied Physics Letters*, vol. 84, no. 20, pp. 3990–3992, 2004.
[7] J. N. Anker, W. P. Hall, O. Lyandres, N. C. Shah, J. Zhao, and R. P. Van Duyne, “Biosensing with plasmonic nanosensors,” *Nat Mater*, vol. 7, no. 6, pp. 442–453, Jun. 2008.
[8] X. Huang, S. Neretina, and M. A. El-Sayed, “Gold Nanorods: From Synthesis and Properties to Biological and Biomedical Applications,” *Advanced Materials*, vol. 21, no. 48, pp. 4880–4910, 2009.
[9] H. A. Atwater and A. Polman, “Plasmonics for improved photovoltaic devices,” *Nat Mater*, vol. 9, no. 3, pp. 205–213, Mar. 2010.
[10] S. J. Lee, Z. Guan, H. Xu, and M. Moskovits, “Surface-Enhanced Raman Spectroscopy and Nanogeometry: The Plasmonic Origin of SERS,” *J. Phys. Chem. C*, vol. 111, no. 49, pp. 17985–17988, Dec. 2007.
[11] K. Aslan, I. Gryczynski, J. Malicka, E. Matveeva, J. R. Lakowicz, and C. D. Geddes, “Metal-enhanced fluorescence: an emerging tool in biotechnology,” *Current Opinion in Biotechnology*, vol. 16, no. 1, pp. 55–62, Feb. 2005.
[12] D.-K. Lim, K.-S. Jeon, H. M. Kim, J.-M. Nam, and Y. D. Suh, “Nanogap-engineerable Raman-active nanodumbbells for single-molecule detection,” *Nat Mater*, vol. 9, no. 1, pp. 60–67, Jan. 2010.
[13] D. Punj, M. Mivelle, S. B. Moparthi, T. S. van Zanten, H. Rigneault, N. F. van Hulst, M. F. García-Parajó, and J. Wenger, “A plasmonic /`antenna-in-box/’ platform for enhanced single-molecule analysis at micromolar concentrations,” *Nat Nano*, vol. 8, no. 7, pp. 512–516, Jul. 2013.
[14] Y. B. Zheng, L. Jensen, W. Yan, T. R. Walker, B. K. Juluri, L. Jensen, and T. J. Huang, “Chemically Tuning the Localized Surface Plasmon Resonances of Gold Nanostructure Arrays,” *J. Phys. Chem. C*, vol. 113, no. 17, pp. 7019–7024, Apr. 2009.
[15] J. B. Jackson and N. J. Halas, “Surface-enhanced Raman scattering on tunable plasmonic nanoparticle substrates,” *PNAS*, vol. 101, no. 52, pp. 17930–17935, 2004.
[16] J. R. Cole and N. J. Halas, “Optimized plasmonic nanoparticle distributions for solar spectrum harvesting,” *Applied Physics Letters*, vol. 89, no. 15, pp. 153120–153120–3, Oct. 2006.
[17] K.-H. Kim and Q-Han Park, “Perfect anti-reflection from first principles,” *Sci Rep*, vol. 3, Jan. 2013.
[18] S. Ji, J. Park, and H. Lim, “Improved antireflection properties of moth eye mimicking nanopillars on transparent glass: flat antireflection and color tuning,” *Nanoscale*, vol. 4, no. 15, pp. 4603–4610, Jul. 2012.
[19] C. Vieu, F. Carcenac, A. Pépin, Y. Chen, M. Mejias, A. Lebib, L. Manin-Ferlazzo, L. Couraud, and H. Launois, “Electron beam lithography: resolution limits and applications,” *Applied Surface Science*, vol. 164, no. 1–4, pp. 111–117, Sep. 2000.
[20] R. D. Piner, J. Zhu, F. Xu, S. Hong, and C. A. Mirkin, “‘Dip-Pen’ Nanolithography,” *Science*, vol. 283, no. 5402, pp. 661–663, 1999.
[21] J. Melngailis, “Focused ion beam lithography,” *Nuclear Instruments and Methods in Physics Research Section B: Beam Interactions with Materials and Atoms*, vol. 80–81, Part 2, pp. 1271–1280, 1993.
[22] J. D. Caldwell, O. Glembocki, F. J. Bezares, N. D. Bassim, R. W. Rendell, M. Feygelson, M. Ukaegbu, R. Kasica, L. Shirey, and C. Hosten, “Plasmonic Nanopillar Arrays for Large-Area, High-Enhancement Surface-Enhanced Raman Scattering Sensors,” *ACS Nano*, vol. 5, no. 5, pp. 4046–4055, May 2011.
[23] C. L. Haynes and R. P. Van Duyne, “Nanosphere Lithography: A Versatile Nanofabrication Tool for Studies of Size-Dependent Nanoparticle Optics,” *J. Phys. Chem. B*, vol. 105, no. 24, pp. 5599–5611, Jun. 2001.
[24] D. Nguyen, D. Taylor, K. Qian, N. Norouzi, J. Rasmussen, S. Botzet, M. Lehmann, K. Halverson, and M. Khine, “Better shrinkage than Shrinky-Dinks,” *Lab Chip*, vol. 10, no. 12, pp. 1623–1626, Jun. 2010.
[25] K. Asakawa and T. Hiraoka, “Nanopatterning with Microdomains of Block Copolymers using Reactive-Ion Etching Selectivity,” *Japanese Journal of Applied Physics*, vol. 41, no. Part 1, No. 10, pp. 6112–6118, 2002.

[26] J. S. Mijovic and J. A. Koutsky, “Etching of Polymeric Surfaces: A Review,” *Polymer-Plastics Technology and Engineering*, vol. 9, no. 2, pp. 139–179, 1977.
[27] B. Päivänranta, H. Merbold, R. Giannini, L. Büchi, S. Gorelick, C. David, J. F. Löffler, T. Feurer, and Y. Ekinci, “High Aspect Ratio Plasmonic Nanostructures for Sensing Applications,” *ACS Nano*, vol. 5, no. 8, pp. 6374–6382, Aug. 2011.
[28] H. Jung and K.-H. Jeong, “Monolithic polymer microlens arrays with antireflective nanostructures,” *Applied Physics Letters*, vol. 101, no. 20, pp. 203102–203102–4, Nov. 2012.
[29] C. L. Cheung, R. J. Nikolić, C. E. Reinhardt, and T. F. Wang, “Fabrication of nanopillars by nanosphere lithography,” *Nanotechnology*, vol. 17, no. 5, p. 1339, Mar. 20